

PAPER

A liver-on-a-chip platform with bioprinted hepatic spheroids

To cite this article: Nupura S Bhise *et al* 2016 *Biofabrication* **8** 014101

View the [article online](#) for updates and enhancements.

Related content

- [Construction of a liver sinusoid based on the laminar flow on chip and self-assembly of endothelial cells](#)
Shengli Mi, Xiaoman Yi, Zhichang Du *et al.*
- [3D liver membrane system by co-culturing human hepatocytes, sinusoidal endothelial and stellate cells](#)
Haysam Mohamed Magdy Ahmed, Simona Salerno, Sabrina Morelli *et al.*
- [Development of a 3D cell printed construct considering angiogenesis for liver tissue engineering](#)
Jin Woo Lee, Yeong-Jin Choi, Woon-Jae Yong *et al.*

Recent citations

- [Advances in Hydrogels in Organoids and OrganonaChip](#)
Haitao Liu *et al*
- [Bone-chip system to monitor osteogenic differentiation using optical imaging](#)
Dmitriy Sheyn *et al*
- [A Human Liver-on-a-Chip Platform for Modeling Nonalcoholic Fatty Liver Disease](#)
Soufian Lasli *et al*

BIOPRINTER

EASY-TO-USE
AFFORDABLE
CUSTOMIZABLE
FULLY FEATURED

**BIOPRINTING.
LIKE NEVER
BEFORE.**

LEARN
MORE

Biofabrication



PAPER

A liver-on-a-chip platform with bioprinted hepatic spheroids

RECEIVED
21 February 2015

REVISED
20 August 2015

ACCEPTED FOR PUBLICATION
28 August 2015

PUBLISHED
12 January 2016

Nupura S Bhise^{1,2}, Vijayan Manoharan^{1,2}, Solange Massa^{1,2,3}, Ali Tamayol^{1,2}, Masoumeh Ghaderi^{1,2}, Mario Miscuglio^{1,2}, Qi Lang^{1,2}, Yu Shrike Zhang^{1,2}, Su Ryon Shin^{1,2,4}, Giovanni Calzone^{1,2}, Nasim Annabi^{1,2,4}, Thomas D Shupe⁵, Colin E Bishop⁵, Anthony Atala⁵, Mehmet R Dokmeci^{1,2} and Ali Khademhosseini^{1,2,4,6}

¹ Biomaterials Innovation Research Center, Department of Medicine, Brigham and Women's Hospital, Harvard Medical School, Boston, MA 02115, USA

² Harvard-MIT Division of Health Sciences and Technology, Massachusetts Institute of Technology, Cambridge, MA 02139, USA

³ Centro de Investigación Biomédica, Universidad de los Andes, Santiago 12445, Chile

⁴ Wyss Institute for Biologically Inspired Engineering, Harvard University, Boston, MA 02115, USA

⁵ Wake Forest Institute for Regenerative Medicine, Wake Forest University School of Medicine, Winston-Salem, NC 27101, USA

⁶ Department of Physics, King Abdulaziz University, Jeddah 21569, Saudi Arabia

E-mail: alik@rics.bwh.harvard.edu

Keywords: bioprinting, bioreactor, liver, drug toxicity, 3D culture, hepatocytes

Abstract

The inadequacy of animal models in correctly predicting drug and biothreat agent toxicity in humans has resulted in a pressing need for *in vitro* models that can recreate the *in vivo* scenario. One of the most important organs in the assessment of drug toxicity is liver. Here, we report the development of a liver-on-a-chip platform for long-term culture of three-dimensional (3D) human HepG2/C3A spheroids for drug toxicity assessment. The bioreactor design allowed for *in situ* monitoring of the culture environment by enabling direct access to the hepatic construct during the experiment without compromising the platform operation. The engineered bioreactor could be interfaced with a bioprinter to fabricate 3D hepatic constructs of spheroids encapsulated within photocrosslinkable gelatin methacryloyl (GelMA) hydrogel. The engineered hepatic construct remained functional during the 30 days culture period as assessed by monitoring the secretion rates of albumin, alpha-1 antitrypsin, transferrin, and ceruloplasmin, as well as immunostaining for the hepatocyte markers, cytokeratin 18, MRP2 bile canalicular protein and tight junction protein ZO-1. Treatment with 15 mM acetaminophen induced a toxic response in the hepatic construct that was similar to published studies on animal and other *in vitro* models, thus providing a proof-of-concept demonstration of the utility of this liver-on-a-chip platform for toxicity assessment.

Introduction

The current drug development process suffers from a high failure rate during clinical trials, which is partly due to inadequacy of animal models to accurately predict the toxic side-effects of drugs in humans [1, 2]. There is a need to develop better predictive platforms that can complement the existing approaches for drug discovery based on preclinical animal models followed by clinical trials [3, 4]. Engineered tissues are being increasingly used to model diseases and for *in vitro* drug testing [5–8]. Advances in the areas of biomaterials and tissue engineering have led to exciting developments towards the goal of generating tissue constructs from human cells that can mimic the endogenous cell–cell and cell–matrix interactions [6].

Moreover, the advances in microfluidic systems allow the fabrication of microbioreactors for growing these engineered tissues under continuous perfusion, and providing cells with various physiological stimuli as well as supplying cells with nutrients and oxygen [9, 10]. Consequently, the concept of organ-on-a-chip and body-on-a-chip has emerged as promising platforms that can be used for studying the effect of drugs and environmental toxins on the targeted and surrounding tissues [11–15]. Organ-on-a-chip platforms will also provide potential avenues for screening biothreat and chemical warfare agents [3].

Liver plays a critical role in drug metabolism and detoxification of blood. Drug-induced hepatotoxicity is one of the main reasons for drug withdrawal, thus highlighting the need for developing a robust *in vitro*

model for evaluating hepatotoxicity [16, 17]. Recent advancements in microfabrication technologies have enabled the creation of architectures that can mimic *in vivo* conditions. For instance, Ho *et al* micro-fabricated centimeter scale morphology of liver lobules and controlled the distribution of hepatocytes and endothelial cells in two-dimensional (2D) culture. They monitored the cellular activity for only 2 days [18]. However, hepatic models that utilize conventional 2D mono- and co-cultures of normal and diseased human cells fail to mimic the complex three-dimensional (3D) *in vivo* microenvironment and extracellular matrix (ECM) support [16, 19, 20]. Thus, it can prevent normal cellular function and response to the tested drugs. To address this challenge, efforts are focused on developing 3D models that can better recapitulate *in vivo* cell–cell, cell-ECM interactions, and the tissue architecture. *Ex vivo* studies using 3D tissue biopsies or slices have been reported, but they may be difficult to be used for high-throughput studies and show rapid loss of functionality within a few days *in vitro*, thus limiting their application for long-term studies [21]. Part of recent approaches have thus focused on encapsulation of cells within hydrogels such as gelatin, poly(ethylene glycol) diacrylate (PEGDA), and agarose, which mimic the physico-chemical characteristics of native ECM [22–24].

Tsang *et al* encapsulated primary rat hepatocytes within 3D PEGDA constructs doped with RGD and cultured them in a flow bioreactor as a liver model for 12 days [24]. Li *et al* achieved the maintenance of liver-specific functionality of rat hepatocyte microtissues embedded within PEGDA for about 50 days, but this study was performed in static culture conditions [25]. Moreover, the use of rat hepatocytes in these studies limited their ability to predict human clinical outcomes. Static cultures that are traditionally used for drug testing lack the physiological cues important for drug metabolism, which has been highlighted in multiple reports [13–15, 26]. Thus, the utilization of physiologically relevant dynamic models, which provide appropriate mass-transport for gas and metabolite waste, becomes imperative for drug toxicity studies [14, 15, 27]. In a study by He *et al*, HepG2 human hepatocarcinoma cells were encapsulated within agarose hydrogel containing planar perfusable channels and continuously perfused with unidirectional flow to form a pre-vascularized liver-like structure [23]. However, they only monitored cellular viability for a 3 day culture period and did not assess liver-specific functionality. Interestingly, Esch *et al* reported that bi-directional fluidic flow enhanced the metabolic activity of multi-cellular 3D hepatic tissue cultured for 14 days as observed with unidirectional flow [27]. Another approach recently reported by Liu *et al* was to apply magnetic field for controlled fabrication of 3D microtissues [28]. Although this approach has shown promising results for fabrication of simple 3D constructs, the fabrication of more complex biomimetic

constructs might be challenging. Limitations with these approaches highlight the need for developing 3D hydrogel-based human liver constructs in microfluidic-based bioreactors amenable for long-term functionality and drug toxicology studies. These platforms reduce the consumption of expensive reagents, allow for temporal control of drug dose, and provide scalability and reproducibility [29].

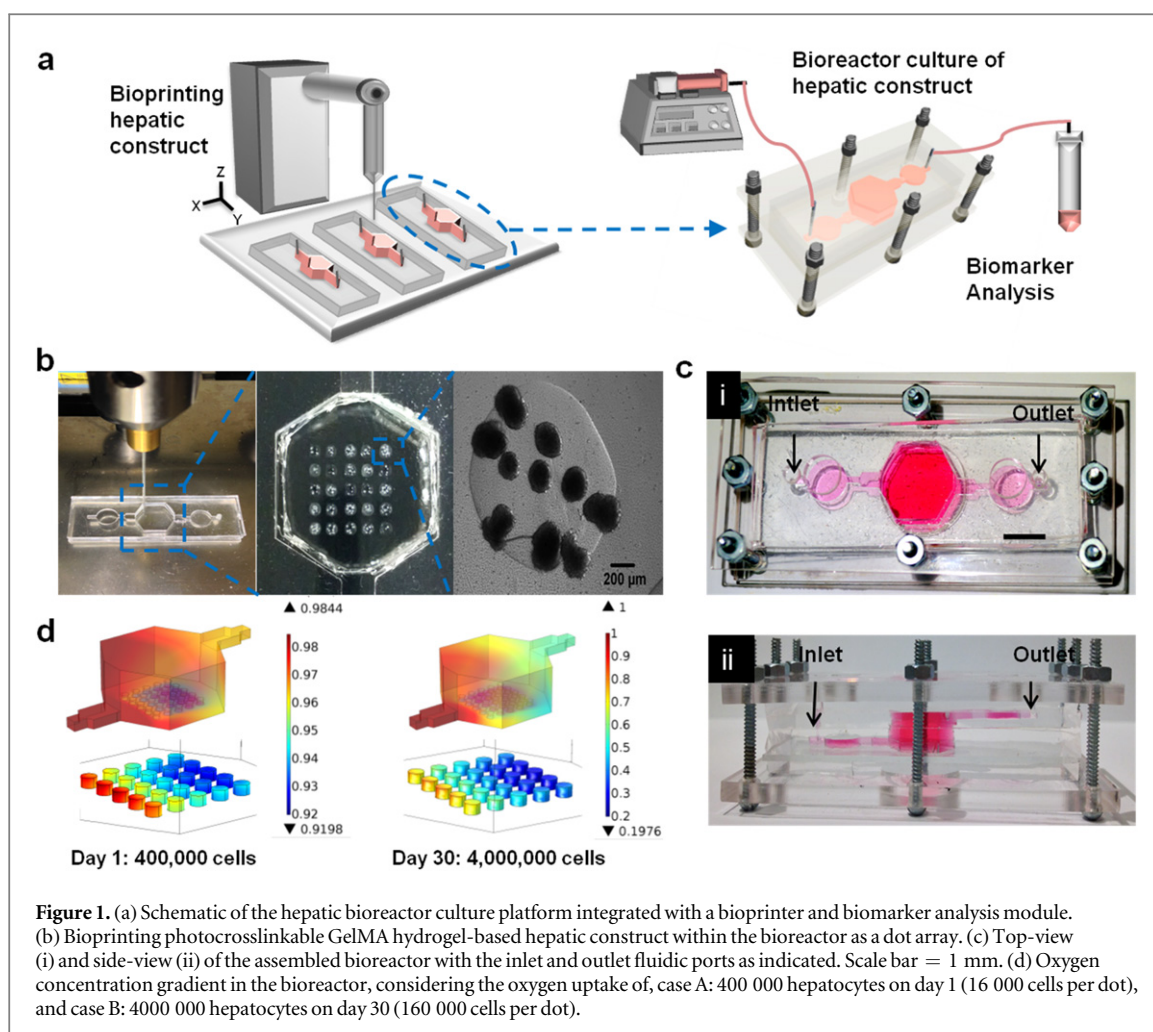
Bioprinting approaches facilitate automated and high-throughput fabrication of precisely controlled 3D architectures [30, 31]. Thus, combining them with miniaturized bioreactors allows the realization of next generation organ-on-a-chip platforms. Moreover, a bioreactor that allows easy access to the hepatic construct within the bioreactor without compromising the construct is highly desirable for assessing tissue behavior at multiple time points during the long-term culture period. Among various 3D cell culture models, multicellular spheroids, formed by aggregation of cells compacted together by self-secreted ECM, have recently been the focus of a number of studies [32–37]. The oxygen tension in the core of the spheroids contrasts with that in the periphery, better mimicking the *in vivo* oxygen gradient in the hepatic lobule [38]. As a result, the use of cell spheroids instead of disperse cells might improve the cellular functionality and response for drug toxicity assessment. Moreover, the encapsulation of cell spheroids within hydrogels that are compatible with rapid fabrication techniques including bioprinting, enables the fabrication of complex architectures similar to those observed *in vivo*.

In this study, we fabricated a perfusable bioreactor that allowed for direct access to cells during the long-term culture period. We interfaced the designed bioreactor with a direct write printer to create HepG2/C3A hepatic spheroid-laden hydrogel constructs. The bioprinted tissue-like constructs were incubated under continuous perfusion, and cellular functionality was assessed over a period of 4 weeks. We also assessed cellular response to acute acetaminophen (APAP) exposure in this bioreactor platform as a model for predictive drug toxicity comparable with *in vivo* conditions.

Materials and methods

Materials

2-Hydroxy-1-(4-(hydroxyethoxy)phenyl)-2-methyl-1-propanone (Irgacure 2959, CIBA Chemicals) was used as photoinitiator (PI) for crosslinking photocrosslinkable gelatin (GelMA) hydrogel. Dulbecco's modified Eagle medium (DMEM), fetal bovine serum (FBS), LIVE/DEAD® Viability/Cytotoxicity Kit for mammalian cells, penicillin/streptomycin antibiotics, 0.05% trypsin-EDTA (1X), and PrestoBlue® cell viability reagent were all purchased from Invitrogen (Life Technologies, Carlsbad, CA, USA). All antibodies and enzyme-linked immunosorbent assay (ELISA) kits



were purchased from Abcam (Cambridge, MA, USA). Other reagents and materials were purchased from Sigma Aldrich (St. Louis, MO, USA) unless mentioned otherwise.

GelMA was synthesized as previously described by functionalizing 10% (w/v) gelatin (G2500, Sigma-Aldrich) in Dulbecco's phosphate buffered saline (DPBS) by the dropwise addition of methacrylic anhydride (276 685, Sigma-Aldrich) [7, 39]. The concentration of methacrylic anhydride in the reaction mixture was 8% (v/v). This reaction was carried out for 2 h at 50 °C with constant stirring at 200 rpm. The reaction was then stopped by dilution with DPBS and dialyzed for 7 days at 40 °C under constant stirring at 500 rpm. The dialyzed solution was sterile filtered and freeze dried for 5 days. The lyophilized foam was stored at room temperature for any future use.

Bioreactor design and fabrication

Figure 1(a) shows the schematic of the overall bioreactor platform utilized in the present study. The designed bioreactor consisted of multilayers of polydimethylsiloxane (PDMS) and poly(methyl methacrylate) (PMMA) and included three chambers connected by fluidic channels as shown in figures S1(a) and (b) in ESI. The chambers and channels were all fabricated

using PDMS by casting PDMS around laser cut PMMA molds. A 3-(trimethoxysilyl)propyl methacrylate coated glass slide was used as the bottom layer and the hydrogel constructs were directly bioprinted on top of it (figure 1(b)). The multilayer design was selected in a way that any introduced bubble would be washed away without getting trapped within the chambers. The PDMS layers and glass slide were sandwiched between two layers of PDMS covered PMMA sheets. Eight sets of screws and nuts were used to compress the layer together to prevent potential leakage (figure 1(c)). Unlike the majority of PDMS-based on-chip systems, which are permanently plasma bonded to seal the compartments, the bioreactor could be unscrewed for disassembly at any time for allowing direct access to the hepatic construct and then resealed.

The central cell culture chamber size was selected to allow it to be interfaced with the employed direct write bioprinter. The dimensions of the chambers and the fluidic channels are all listed in figure S1. The total volume of the system was estimated to be 2.4 mL. Upon the completion of the bioprinting process (explained later), the bioreactor was connected to a syringe pump (Harvard Apparatus PhD 2000, Cambridge, MA, USA) and was perfused with media

continuously. A 60 mL plastic syringe (Becton Dickinson and Company, East Rutherford NJ, USA) was filled with the HepG2/C3A culture medium. A 27 G 1/2 needle (Becton Dickinson and Company, East Rutherford, NJ, USA) was connected to the syringe and subsequently 30 cm of tubing (Cole-Palmer #30 AWG thin wall tubing natural, Veron Hills, IL, USA) was used to connect the syringe to the inlet port of the bioreactor. The outlet tubing of the bioreactor was connected to a 50 mL reservoir tube to collect culture media for biomarker analysis.

Numerical simulations

Hepatocytes are known to be responsive to oxygen concentration and the exposed shear stress. To determine the flow rate that ensures sufficient oxygen concentration within the cell culture chamber specially at the vicinity of the hydrogel constructs, COMSOL Multiphysics (COMSOL Inc.) was used to estimate the oxygen and flow fields. Standard transport equations were used in the simulations. In particular, Navier Stokes equations with no slip boundary condition and convection–diffusion equation were used for modeling of flow and oxygen transport in channels and chamber. Although PDMS is oxygen permeable [40], since the bioreactor is covered by a impermeable PMMA layer, we considered the worst case scenario and all boundaries were treated as impermeable surfaces. The transport properties of the spheroids are not well understood in the literature, thus, could not be incorporated within the theoretical simulation. The hydrogels were modeled as a porous media with uniform volumetric oxygen consumption rate associated with the total number of encapsulated cells. Volume averaged equations were used for modeling the transport equations in the porous hepatic constructs. The oxygen concentration at the inlet was considered to be constant and uniform. The oxygen consumption of HepG2/C3A cells can be described with the Michaelis–Menten kinetics [41, 42]:

$$R_{O_2} = V_{\max} \frac{c_{O_2}}{c_{O_2} + k_{MM,O_2}} \delta(c_{O_2} > c_{cr}), \quad (1)$$

where, V_{\max} is the maximum volumetric oxygen consumption rate ($\text{mol m}^{-3} \text{s}^{-1}$) and depends not only on the volumes but also on the concentration of cells in the bioreactor, c_{O_2} is the oxygen concentration in the cell layer and k_{MM,O_2} is the Michaelis constant.

$$V_{\max} = \frac{q N_{\text{cells}}}{V}, \quad (2)$$

where, q represents the oxygen consumption per cell, its value is $4.76 \times 10^{-16} \text{ mol s}^{-1}$, N_{cells} is the number of cell, and V the volume of the hepatic construct in the bioreactor [43]. Moreover, a value of $6.3 \times 10^{-3} \text{ mol m}^{-3}$ was considered for k_{MM,O_2} . To exclude the effect of dead cells from oxygen consumption rate, a heaviside function was implemented The c_{cr} , the critical limit at which cells die due to hypoxia,

was considered to be $1.0 \times 10^{-4} \text{ mol m}^{-3}$ [42]. The diffusion coefficient of oxygen in aqueous media at 37°C was assumed as a reasonable approximation of $3.8 \times 10^{-9} \text{ m}^2 \text{ s}^{-1}$. An unstructured 3D numerical grid was used throughout the analysis and the governing equations were solved by a segregated solver. The grid independence of the results was checked and we noticed that a grid size of 800 000 nodes provides grid independent results.

Cell culture

HepG2/C3A cells (ATCC) were maintained in DMEM 1X medium with 10% FBS and incubated at 37°C with 5% CO_2 . Medium was renewed every 48 h.

Spheroid formation using PDMS microwells

A negative silicon mold containing posts (200 μm in diameter) was created using standard lithography technique [44]. The PDMS replica against the silicon wafer was formed by casting the PDMS in a mixture of 10:1 silicon elastomer and the curing agent (Sylgard 184, Dow Corning, Midland, MI, USA). The blend was then degassed and cured for 1 h at 80°C , and the PDMS mold was formed. After trypsinization, HepG2/C3A cells were seeded at a concentration of 8×10^6 cells in 7 mL media per PDMS mold, the cells were allowed to settle in the wells by gravity for 1 to 2 h, following which media was aspirated carefully and fresh media was added to the mold. The cells were kept in incubation with a daily supply of fresh media for 5 days till spheroids were formed. On day 5 spheroids were harvested and collected for encapsulation and bioprinting.

Bioprinting of hepatic constructs containing 3D hepatic spheroids

The harvested spheroids were mixed with a solution containing 10% (w/v) GelMA and 0.5% (w/v) 2-hydroxy-4'-(2-hydroxyethoxy)-2-methylpropio-phenone (410896, Sigma-Aldrich) in DPBS. A 7×7 array was then printed as liquid droplets from this mixture on a glass slide within the cell culture chamber of the bioreactor using a NovoGen MMX Bioprinter TM (Organovo, San Diego, CA, USA) whose operation is described elsewhere [45]. In brief, the bioprinter used a hollow capillary and piston system augmented with an automated X – Y – Z stage to print the solution loaded in it. The bioprinted solution of spheroids and GelMA were then crosslinked by immediate UV light illumination with an intensity of 850 mW from a distance of 8.5 cm for a period of 15 s.

Hepatic biomarker concentration

The media samples from the bioreactor cultures were collected on days 1, 7, 15, 21 and 30 at the fluidic outlet port. Secreted albumin, ceruloplasmin, alpha-1 anti-trypsin (A1AT) and transferrin in the supernatant were measured by human ELISA kits (Abcam, Cambridge, UK). The media was collected for a period of

24 h at each time point and the average biomarker concentration (ng mL^{-1}) in the bulk media was measured using ELISA. This concentration (ng mL^{-1}) was used to calculate the secretion rates (ng h^{-1}) of the four biomarkers during the 24 h period.

Cell count

To count the number of cells cultured per bioreactor, the hepatic hydrogel samples were treated with collagenase (1 mg mL^{-1}) at 37°C for 10 min until the GelMA hydrogel fully degraded. After adding culture media, cells were centrifuged and treated with 2X trypsin at 37°C for 5 min. The cell suspension was centrifuged again, the pellet was dispersed in culture media and cells were counted using a hemocytometer.

Immunostaining

The encapsulated spheroids were immunostained for observing the protein expression of markers, ZO-1, cytokeratin 18 and multidrug resistance-associated protein 2 (MRP2) on day 30. All antibodies were purchased from Abcam, Cambridge, UK. For drug studies the samples were analyzed after 7 days of culture. Briefly, the samples were fixed with 4% (v/v) paraformaldehyde and then treated with 0.1% (v/v) triton. Then, the samples were blocked with 10% (v/v) goat serum and incubated overnight at 4°C with primary antibodies at a dilution of 1:50 for ZO-1 (ab59720), 1:200 for cytokeratin 18 (ab7797) and 1:100 for MRP2 (ab3373). The samples were washed with DPBS and incubated for 1 h with secondary antibodies at a dilution of 1:200. The samples were then treated with DAPI (1:1000) for 10 min at 37°C and washed briefly with DPBS before imaging.

Microscopy

The immunostained samples were imaged using an inverted laser-scanning confocal microscope (Olympus FV1200, Center Valley, PA, USA). For phase contrast images, an inverted Zeiss D1 observer microscope (Oberkochen, Germany) was used. For real-time monitoring of the growth of the spheroids in the bioreactors, we utilized a commercially available miniature microscope, JuLI Br (NanoEnTek USA Inc., Pleasanton, CA, USA) live cell movie analyzer with a small custom modification to adjust the working distance of the objective.

Cellular metabolic activity assay

To assess cellular metabolic activity, Presto Blue Reagent (Life Technologies, Carlsbad, CA, USA) was used in static conditions. Every two days media from the culture was removed and the spheroids were incubated for 3 h at 37°C with Presto Blue assay. Fluorescence was measured at 560 nm(ex)/590 nm(em) in control and different APAP concentrations to evaluate hepatotoxicity of the drug.

Drug (acetaminophen) treatment

For static dose-response experiments, spheroids were encapsulated in GelMA and bioprinted onto glass slides grafted with 3-(trimethoxysilyl) propyl methacrylate. Each glass slide was then placed into a well of a 6 well plate and spheroids were cultured in phenol red free media for 24 h. After 24 h, the GelMA embedded spheroids were exposed to 0, 1, 5, 10 or 20 mM of acetaminophen (APAP, Sigma-Aldrich) for 48 h in static condition. For the dynamic bioreactor experiments, the GelMA embedded spheroids bioprinted in the bioreactor were exposed continuously to a 15 mM dose of APAP at $200 \mu\text{L h}^{-1}$ for 7 days. Media was replaced every two days and Presto Blue assay was carried out after each media removal.

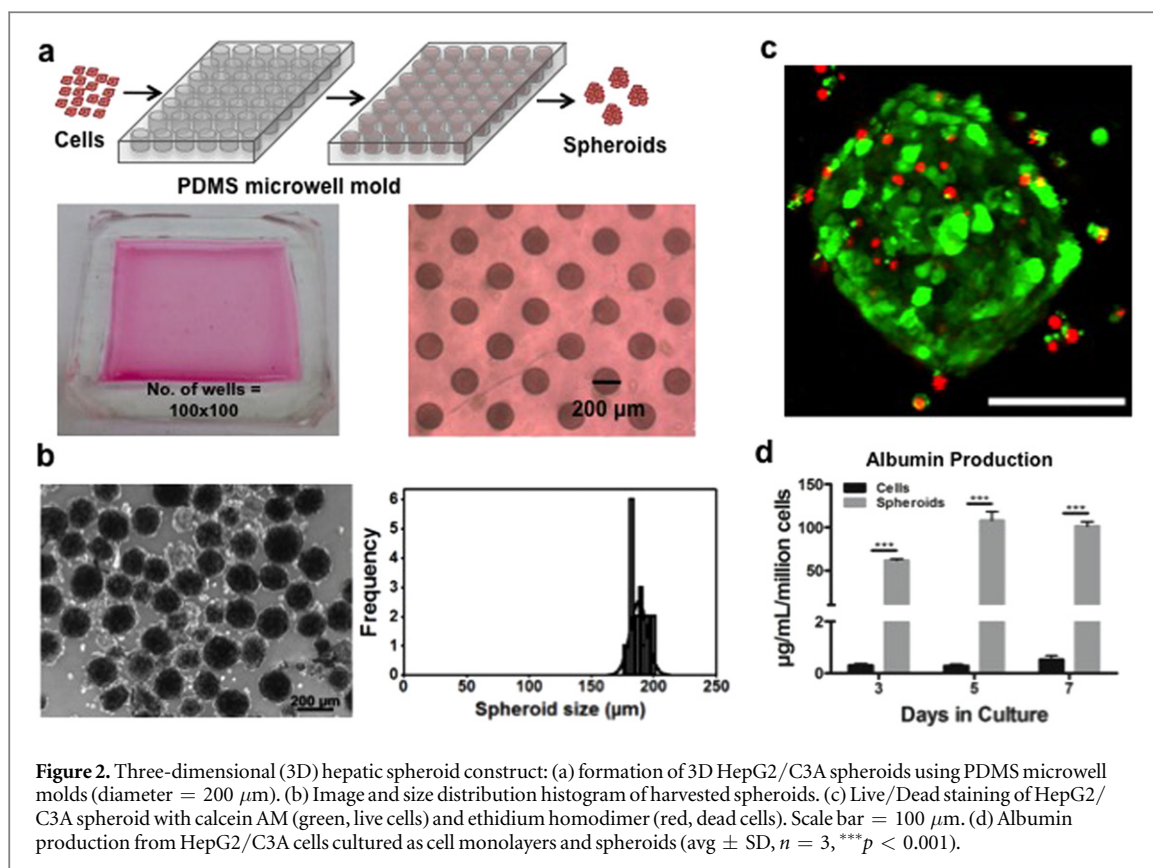
Statistical analysis

Data is plotted as average (avg) \pm standard deviation (SD) using Graph Pad Prism software. Two-way ANOVA and a Tukey's post-hoc test was used to compare data (* $p < 0.05$, ** $p < 0.01$, and *** $p < 0.001$).

Results and discussion

Bioreactor platform overview

The fabricated bioreactor shown in figure 1(c) was interfaced with a bioprinter to incorporate 3D cell-laden hydrogel constructs. Moreover, the resealability of the design allowed direct access to the cells during the experiment for biological analysis. Although use of high volumetric flow rates can ensure sufficient oxygen and nutrient presence within the bioreactor, the concentration of biomarkers secreted by the cells may get too diluted, interfering with monitoring cellular response to drugs and toxins. Thus, we planned to determine the minimum flow rate that guarantees sufficient oxygen concentration at the vicinity of the hydrogel constructs. We performed numerical simulations at flow rates ranging from 100 to $1000 \mu\text{L h}^{-1}$. Figure S1 shows the bioreactor dimensions, wherein the volume of the main cell chamber was about 2 mL and the channel volume was about $350 \mu\text{L}$. The following parameters were considered in these simulation: media viscosity = 1.1 mPa s^{-1} , oxygen diffusivity = $3.8 \times 10^{-8} \text{ m}^2 \text{ s}^{-1}$, and $V_{\text{max}} = 4.76 \times 10^{-16} \text{ mol s}^{-1}$ [43]. The cell count from bioprinted constructs cultured in the bioreactor for 30 days showed that the cell number per bioreactor increased from $4 \pm 0.5 \times 10^5$ cells on day 1 to $4 \pm 0.2 \times 10^6$ cells on day 30. From the numerical simulations using these two cell numbers, we found that the minimum c_{O_2} at any point within the chamber was 91% of the inlet value at day 1 for a flow rate of $200 \mu\text{L h}^{-1}$ (figure 1(d)). This value dropped to an average of 38% (minimum 19%) at day 30. Thus, a flow rate of higher than $200 \mu\text{L h}^{-1}$ allowed for sufficient c_{O_2} for hepatocytes ($1.0 \times 10^{-4} \text{ mol m}^{-3}$) [42]. As a result, the flow rate of $200 \mu\text{L h}^{-1}$ was used throughout the experiments.



Hepatic spheroid formation

A high-throughput PDMS microwell technique was used to form hepatic spheroids as shown in figure 2(a). HepG2/C3A cells were seeded into a microwell array mold (each well: 200 μm diameter and 200 μm height) and harvested after 5 days of culture. A batch of 10 000 spheroids was obtained per mold. The average size was estimated to be $191 \pm 10 \mu\text{m}$ by measuring the size of ~ 30 spheroids (figure 2(b)). To calculate the size of the individual spheroids shown in the graph, the spheroids were harvested in a petri dish, imaged with a Nikon Eclipse Ti inverted microscope and the images were analyzed using SPOT imaging solutions software using the area (diameter) automatic calculation tool. In the picture of the spheroids (figure 2(b)), the distribution is slightly greater than the graph because a few spheroids that were not densely aggregated as indicated by a lighter shade and easily broke into smaller pieces ($< 150 \mu\text{m}$) by the force applied during harvesting were not included while counting the diameter. Similar to these smaller spheroid pieces, there were extremely few aggregates with diameter slightly greater than 200 μm in the samples, as indicated by the graph. The spheroid size could be easily adjusted by tuning the microwell size. Literature suggests that a size of 200 μm is suitable to avoid necrosis in the core, while maintaining the functionality of the cells within the spheroids [46, 47]. We confirmed the cell viability in the spheroids harvested after 5 days of microwell

culture using Live/Dead staining. The Z-stack confocal microscope image of the stained spheroid showed viable cells (green, Calcein AM) in the core of the spheroid (figure 2(c)). In addition, we compared the albumin production from spheroid and cell monolayer culture in static conditions (figure 2(d)). The albumin production ($\mu\text{g}/\text{mL}/\text{million cells}$) was significantly higher from spheroids, 101 ± 5.2 on day 7, as compared to cell monolayers, 0.5 ± 0.1 on day 7, during the 7 days culture period. Increased albumin secretion from spheroids compared to cell monolayers, as seen here, is consistent with observations reported in literature, which indicates that culturing the cells as spheroids may enhance homotypic cell–cell interactions within aggregated hepatocytes and improve functional outcomes of the hepatic construct [25, 48]. HepG2 cells can cluster over time, but dispersed cells take longer to form these cell–cell interactions when encapsulated in a porous scaffold compared to spheroids, which could affect their resistance to drugs [49].

Bioprinting hydrogel-based hepatic constructs in the bioreactor

Interfacing bioreactors and 3D bioprinters bring the opportunity of fabricating sophisticated constructs in the future, which is one of the challenges in organ-on-a-chip field. Thus, we designed the system in a way that it supports the bioprinter and bioreactor interfacing.

For bioprinting of the hepatic construct, we used GelMA hydrogel, which is a bioresponsive and biodegradable ECM derived hydrogel [50]. We bioprinted dot-arrays of the prepolymer GelMA hydrogel solution mixed with spheroids fabricated using micromolds ($40\,000$ spheroids mL^{-1}) as shown in figure 1(b). The central cell culture chamber dimensions (figure S1) were selected to allow it to be interfaced with the employed direct write bioprinter. As seen in the side view micrograph of the bioprinted hydrogel with spheroids in figure S2, the thickness of the bioprinted GelMA dot is $\sim 800\ \mu\text{m}$, which is thicker than the average diameter of the spheroids ($\sim 200\ \mu\text{m}$). Moreover, the dimensions of the bioprinted hydrogel features were much smaller than the 8 mm depth of the chamber. The thickness of the hydrogel dot can be tuned by modifying the diameter of the capillary and piston in the bioprinter and printing time. By adapting this method, we avoided potentially harsh printing conditions including, low temperature for a prolonged printing period [51] and undesirable shear stress along the length of the nozzle [30]. The use of bioprinting in our system not only paved the way for a rapid fabrication of the 3D hepatic construct, but also allowed for a precise control over the thickness of the hydrogel layer encapsulating the spheroids to maintain consistency in mass diffusion through the hydrogel, for all experiments. Also, this bioprinting approach enabled easy tailoring of other printing parameters such as spheroid concentration per dot and hydrogel composition, as well as controlling multicellular distribution and the geometrical features of the printed construct. This technique can be further extended to create complex architectural features and consistently control the distribution of multiple hepatic cell types in precise locations. The GelMA concentration (10% w/v of GelMA with $\sim 75\%$ nominal degree of methacrylamide modification [52]) and cross-linking conditions (0.5% w/v PI, 15 s UV exposure with 850 mW intensity and 8.5 cm distance) for the hydrogel were selected since these conditions resulted in an elastic modulus of ≤ 5 kPa [30] is close to the value for liver (~ 1 kPa) [53] to better support cells during a long-term culture period. Although cell secreted proteins interact with the porous hydrogel scaffold, we used the same encapsulation conditions for control and experimental groups, so that these conditions did not affect the results.

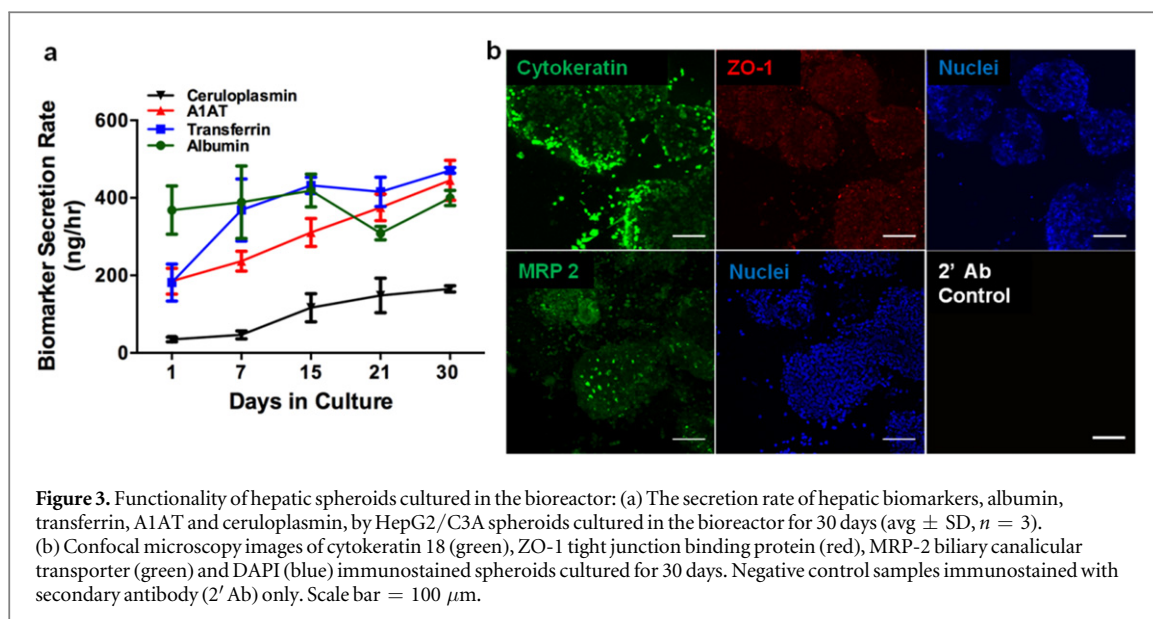
Functionality of hepatic spheroids cultured in the bioreactor

Maintaining the functionality of the hepatic construct in the bioreactor is critical for its application as a drug-testing platform. Freshly isolated or cryopreserved primary hepatocytes are the preferred cell source for drug metabolism studies [54–56]. However, liver-specific functions of primary hepatocytes relevant for

drug development and toxicity studies are rapidly downregulated during their *in vitro* cultures [57]. In addition to their limited lifespan, difficulty in obtaining the cell source and large batch-to-batch variability post-isolation are other important challenges associated with the use of primary hepatocytes. Commercial cell lines including HepG2/C3A provide a more stable, easy-to-handle and readily available source of human cells for *in vitro* studies on liver function and general mechanisms of toxicity [58, 59]. These cell lines offer a reliable alternative to primary cells by overcoming the above issues, especially for use in proof-of-concept studies in dynamic flow liver-on-a-chip platforms [20]. Thus, we used HepG2/C3A based 3D construct for our liver-on-a-chip platform. Although, these cell lines may not express all metabolic enzymes and cannot capture the genetic variability of the patient population, the developed platform paves the path toward engineering constructs from patient-specific hepatocytes derived from induced pluripotent stem cells (iPSCs), which hold great potential for clinical applications [60].

To assess the ability of the bioreactor environment to sustain hepatic functions over a long-term culture period, we bioprinted HepG2/C3A spheroids encapsulated in GelMA in the bioreactor and cultured the construct under continuous perfusion at $200\ \mu\text{L h}^{-1}$ for 30 days. The functionality of the hepatic construct was evaluated by monitoring the concentration of four biomarkers (albumin, A1AT, transferrin, and ceruloplasmin) secreted by the hepatic construct, at different time points: days 1, 7, 15, 21 and 30 (figure 3(a)). The bioreactor culture environment was able to sustain the biomarker production over the course of 30 days. The albumin production from the bioreactor construct was $368 \pm 62\ \text{ng h}^{-1}$ on day 1 and $400 \pm 19\ \text{ng h}^{-1}$ on day 30, transferrin production increased from $181 \pm 48\ \text{ng h}^{-1}$ to $471 \pm 7\ \text{ng h}^{-1}$, A1AT steadily increased from $185 \pm 33\ \text{ng h}^{-1}$ to $445 \pm 52\ \text{ng h}^{-1}$ and ceruloplasmin from $35 \pm 6\ \text{ng h}^{-1}$ to $165 \pm 8\ \text{ng h}^{-1}$. The metabolic activity and function of cells fluctuate over time and similar observations have been reported in the literature [61, 62]. Thus, we speculate that the drop in albumin secretion at day 21 was possibly due to the fluctuation in cellular activity. However, the variations were not statistically significant.

The number of cells per bioreactor was determined to calculate the albumin concentration in terms of pg/cell/day to compare the functionality of the developed liver-on-a-chip platform with previously reported hepatic models. The cell number increased from $4 \pm 0.5 \times 10^5$ cells on day 1 to $4 \pm 0.2 \times 10^6$ cells on day 30, which is a typical cell density range for hydrogel encapsulation [7]. The albumin secreted by the cells (pg/cell/day) in the bioreactor was 20 ± 3 on day 1, 8 ± 2 on day 7, 5 ± 0.5 on day 15, 2.5 ± 0.1 on day 21 and 2.3 ± 0.1 on day 30. This shows that although the relative albumin secreted per cell

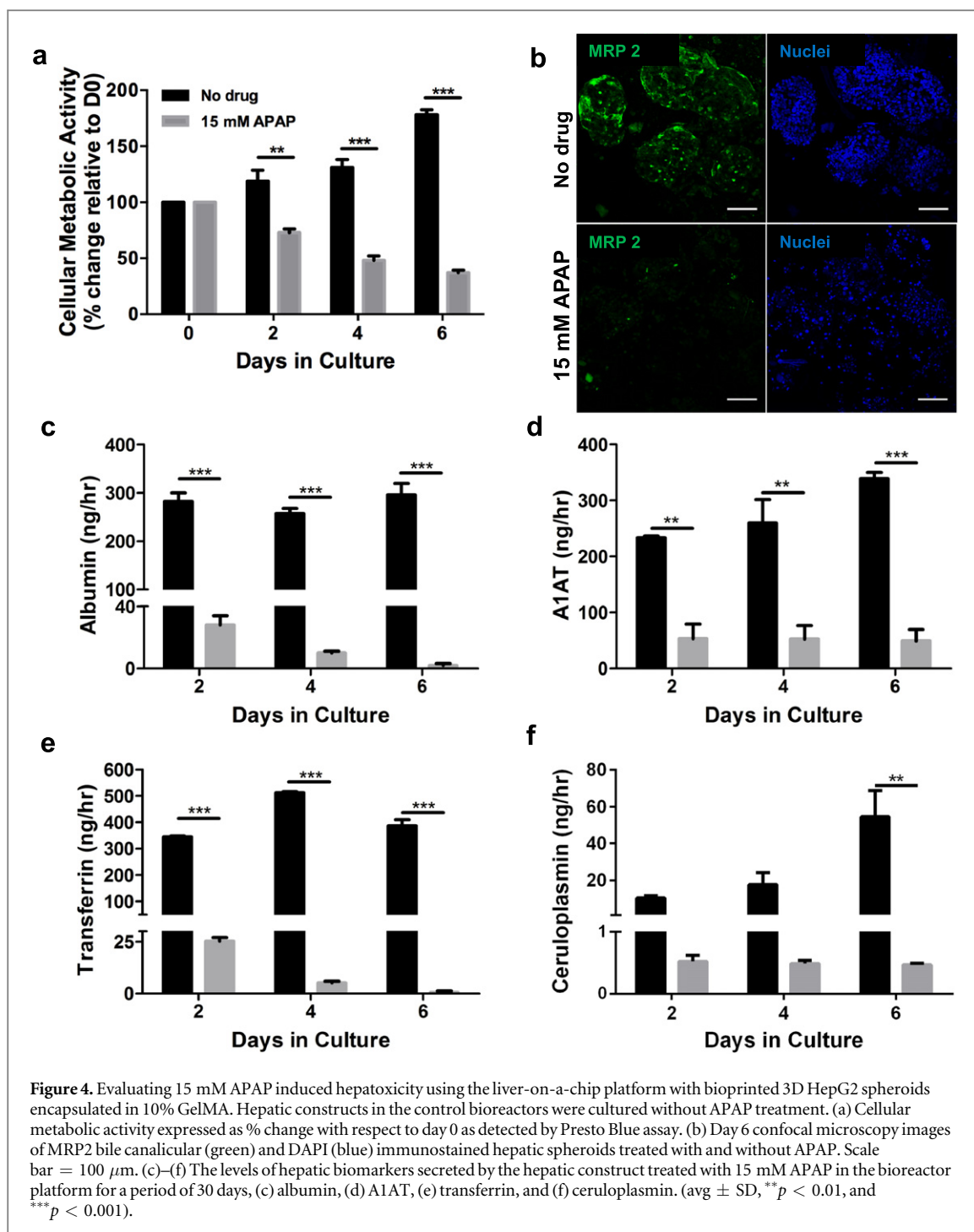


decreased overtime, the level was sustained within the range (0.6–80 pg/cell/day) reported in the literature for albumin production per cell by HepG2 cells/spheroids [63, 64]. Similarly, the amount of A1AT secreted per cell (pg/cell/day) decreased from 10 ± 2 on day 1 to 2.6 ± 0.3 on day 30, the amount of transferrin (pg/cell/day) decreased from 10 ± 2.7 on day 1 to 2.7 ± 0.05 on day 30 and the amount of ceruloplasmin (pg/cell/day) decreased from 2 ± 0.3 on day 1 to 0.95 ± 0.05 on day 30. As in the case of albumin, the levels of these biomarkers were also comparable to the range reported in the literature for A1AT (5–150 pg/cell/day) [65, 66], transferrin (0.1–17.2 pg/cell/day) [65, 67, 68] and ceruloplasmin (0.1–0.7 pg/cell/day) [68] secreted by HepG2 cells. The decrease in production maybe attributed to the decreasing oxygen availability within the spheroid core overtime as the spheroid size increased with cell proliferation (figure S3), without any change in the media perfusion rate ($200 \mu\text{L h}^{-1}$) over the 30 days culture period. Increasing the perfusion rate or reducing the size of spheroids at the start of culture period to compensate for the oxygen deprivation within the spheroid core could potentially increase the cellular activity over long-term culture periods.

We further examined the expression patterns of non-secreted cellular proteins by immunostaining the constructs (figure 3(b)). These include: cytokeratin 18, an important cytoplasmic filament protein in human hepatocytes [69], ZO1, a tight junction protein that enables intercellular communication in 3D hepatic spheroids [70], and MRP2, the biliary canalicular transporter protein in hepatocytes [70]. As shown in figure 3(b), the expression of these hepatic proteins was sustained for 30 days of culture, indicating the bioactivity of hepatocytes during the long term bioreactor culture.

Acute drug toxicity assessment using the bioreactor platform

APAP overdose is a common cause of acute liver failure in the US [71, 72]. Moreover, APAP is a well-characterized hepatotoxic drug and its *in vivo* model data is available in literature [73]. Thus we chose APAP as a model drug to evaluate the drug testing capability of our platform. The goal for the APAP treatment experiment was to test the effectiveness of the developed liver-on-a-chip platform for drug toxicity assessment and thus we aimed to recreate the acute APAP hepatotoxicity scenario. To determine the LC50 (50% viability relative to day 0) of APAP at day 6 in our system, we obtained a dose response curve in static conditions using Presto Blue assay to monitor cellular metabolic activity as shown in figure S4. A concentration range of 0 mM–20 mM of APAP was selected based on LC50 values reported in literature for hepatotoxicity [73]. From the dose response curve, a concentration of 15 mM was selected to induce acute APAP toxicity in the bioreactor culture and the functionality of the construct was monitored over 6 days of culture at multiple time-points. Figure 4(a), shows the percent change in cellular metabolic activity upon exposure of the bioreactor hepatic construct to 15 mM APAP for 6 days (values are normalized to day 0). While the metabolic activity steadily increased in the bioreactor condition without APAP treatment, there was significant decrease in metabolic activity in the bioreactor cultures treated with APAP. The metabolic activity decreased by $63 \pm 2\%$ on day 6 compared to day 0 for the APAP treated bioreactor cultures, whereas for no drug control the metabolic activity increased by $78 \pm 4\%$ as compared to day 0 (figure 4(a)). There were no issues encountered while carefully disassembling and reassembling the platform during this assessment. Immunostaining data of non-treated and APAP treated cultures (figure 4(b)) at day 6



shows that the expression of MRP2 in drug treated cultures decreased as a result of loss of normal cellular activity within the spheroids. The DAPI staining showed the decreased nuclei density within the treated constructs. The production rate of the four biomarkers, albumin (figure 4(c)), A1AT (figure 4(d)), transferrin (figure 4(e)), and ceruloplasmin (figure 4(f)), also significantly decreased over time for the APAP treated cultures as compared to no drug control cultures. The acute hepatotoxic dose of APAP causes apoptosis of HepG2 cells within GelMA encapsulated

spheroids, leading to a decrease in the biomarkers secretion levels in the bioreactor system over time, thus showing that the bioreactor responds to the acute toxic drug dose. In a correlation study by Fey *et al*, the authors reported that the observed trend in the metabolic response of 3D spheroids of immortalized hepatocytes to APAP had a reasonably good correlation with *in vivo* APAP toxicity data, thus showing the utility of HepG2 spheroids for APAP toxicity evaluation in the concentration range that we used for our study [73]. These results suggest the

promise of the developed liver-on-a-chip platform for evaluating acute drug toxicity as a complementary tool during the preclinical animal phase of drug development.

The metabolic functions of the liver are highly dependent on its microstructural architecture, fluid flow patterns, zonal ECM composition, and biochemical (oxygen concentration) gradients [74]. Moreover, supportive interactions with non-parenchymal cells, particularly the vascular, stromal and immune cell types, are important for maintaining the high proliferative capacity of hepatocytes in 3D cultures [75]. The successful interfacing of a bioprinting platform with the bioreactor, as reported here, might allow for the creation of advanced biomimetic architectures by precisely mimicking the distribution of different ECM-like biomaterials, key hepatic tissue cell types including hepatocytes, stellate, endothelial, and Kupfer cells, and their ratios. The use of immortalized cell lines offers a cheap and robust platform for initial toxicity evaluation of an array of drug candidates. We used hepatic spheroids containing immortalized HepG2 cells and did not use primary hepatocytes and other non-parenchymal cells, as our goal was to evaluate the functionality of the bioreactor platform rather than establishing a conclusive close correlation with an *in vivo* model. For advanced metabolic studies, hepatic constructs with primary hepatocytes, which have higher metabolic activity, should be employed to validate the drug toxicity data. The employed bioprinting approach and the designed bioreactor is robust for extending the hepatic construct to primary cells in mono-culture and co-cultures with other parenchymal cell types to move towards more biomimetic liver-on-a-chip platforms. However, issues with cost, availability and batch-to-batch variability make primary hepatocytes a challenging cell source to use. Advances in sources of hepatocytes are crucial for realizing the full potential of next generation liver-on-a-chip platforms for personalized drug screening, disease modeling and therapies. Patient-specific hepatocytes derived from autologous iPSCs have recently emerged as an attractive alternative that can overcome these issues [60]. These iPSC-derived hepatocyte-like cells are still in nascent stages of development and show characteristics similar to fetal hepatocytes [76]. Further developmental studies are needed to yield cells with phenotype and functions similar to those of mature hepatocytes, including drug metabolism, bile formation, and production of blood clotting factors and glucose. In the future, banking of these cells derived from individuals representing the genetic variation of the population would enable advanced high-throughput drug screening platforms. Coupling the media circuit of the liver-on-a-chip platform with other organ models would allow recreating the complex crosstalk between multiple organs that affects drug metabolism and toxicity response at the systemic level [77, 78].

Conclusion

Here, we developed a liver-on-a-chip platform that enabled bioprinting of hepatocyte spheroid-laden hydrogel constructs directly within the culture chamber of a bioreactor. The bioreactor could be easily disassembled to access the cells for biological assessment during the long-term culture period. Numerical simulations were carried out to determine the minimum required flow rate for maintaining sufficient oxygen concentration within the bioreactor. Moreover, analyzing the concentration of secreted biomarkers including albumin, A1AT, transferrin, and ceruloplasmin allowed for monitoring the hepatic functionality of the cultured construct. Cultured spheroids remained viable and active during the 30 days of culture period. The response of the liver-on-a-chip platform to APAP treatment was similar to animal and *in vitro* models, which confirms the possibility of its application for drug toxicity analysis. The proposed concept of a bioreactor interfaced with bioprinters expands the field of organ-on-a-chip and may be a key step towards the fabrication of automated systems for high throughput drug screening.

Acknowledgments

The authors acknowledge funding from the Defense Threat Reduction Agency (DTRA) under Space and Naval Warfare Systems Center Pacific (SSC PACIFIC) Contract No. N66001-13-C-2027, the National Science Foundation (EFRI-1240443), and the National Institutes of Health (EB012597, AR057837, DE021468, HL099073, AI105024, AR063745). The publication of this material does not constitute approval by the government of the findings or conclusion herein. The authors acknowledge the JuLI Br microscopy support from NanoEnTek USA Inc, Pleasanton, CA, USA.

Notes

The authors declare no conflict of interest.

Electronic Supplementary Information (ESI) available: figures showing details of bioreactor design (figure S1), side view of bioprinted pseudo 3D construct (figure S2), increase in spheroid size during culture (figure S3) and APAP dose response curve (figure S4). See DOI: 10.1039/b000000x/

References

- [1] van Midwoud P M, Verpoorte E and Groothuis G M 2011 Microfluidic devices for *in vitro* studies on liver drug metabolism and toxicity *Integr. Biol. (Camb.)* **3** 509–21
- [2] Kaplowitz N 2005 Idiosyncratic drug hepatotoxicity *Nat. Rev. Drug Discovery* **4** 489–99
- [3] Bhatia S N and Ingber D E 2014 Microfluidic organs-on-chips *Nat. Biotechnol.* **32** 760–72
- [4] Ghaemmaghami A M, Hancock M J, Harrington H, Kaji H and Khademhosseini A 2012 Biomimetic tissues on a chip for drug discovery *Drug Discovery Today* **17** 173–81

- [5] Khademhosseini A, Vacanti J P and Langer R 2009 Progress in tissue engineering *Sci. Am.* **300** 64–71
- [6] Bajaj P, Schweller R M, Khademhosseini A, West J L and Bashir R 2014 3D biofabrication strategies for tissue engineering and regenerative medicine *Annu. Rev. Biomed. Eng.* **16** 247–76
- [7] Akbari M et al 2014 Composite living fibers for creating tissue constructs using textile techniques *Adv. Funct. Mater.* **24** 4060–7
- [8] Tamayol A, Akbari M, Annabi N, Paul A, Khademhosseini A and Juncker D 2013 Fiber-based tissue engineering: progress, challenges, and opportunities *Biotechnol. Adv.* **31** 669–87
- [9] Whitesides G M 2006 The origins and the future of microfluidics *Nature* **442** 368–73
- [10] Annabi N et al 2013 Hydrogel-coated microfluidic channels for cardiomyocyte culture *Lab Chip* **13** 3569–77
- [11] Baker M 2011 A living system on a chip *Nature* **471** 661–5
- [12] Lee J B and Sung J H 2013 Organ-on-a-chip technology and microfluidic whole-body models for pharmacokinetic drug toxicity screening *Biotechnol. J.* **8** 1258–66
- [13] Huh D, Matthews B D, Mammoto A, Montoya-Zavala M, Hsin H Y and Ingber D E 2010 Reconstituting organ-level lung functions on a chip *Science* **328** 1662–8
- [14] Bhise N S et al 2014 Organ-on-a-chip platforms for studying drug delivery systems *J. Control Release* **190** 82–93
- [15] Polini A, Prodanov L, Bhise N S, Manoharan V, Dokmeci M R and Khademhosseini A 2014 Organs-on-a-chip: a new tool for drug discovery *Expert Opin. Drug Discovery* **9** 335–52
- [16] Khetani S R and Bhatia S N 2008 Microscale culture of human liver cells for drug development *Nat. Biotechnol.* **26** 120–6
- [17] Yip D and Cho C H 2013 A multicellular 3D heterospheroid model of liver tumor and stromal cells in collagen gel for anti-cancer drug testing *Biochem. Biophys. Res. Commun.* **433** 327–32
- [18] Ho C T et al 2013 Liver-cell patterning lab chip: mimicking the morphology of liver lobule tissue *Lab Chip* **13** 3578–87
- [19] Bhatia S N, Balis U J, Yarmush M L and Toner M 1999 Effect of cell–cell interactions in preservation of cellular phenotype: cocultivation of hepatocytes and nonparenchymal cells *FASEB J.* **13**(14) 1883–900
- [20] LeCluyse E L, Witek R P, Andersen M E and Powers M J 2012 Organotypic liver culture models: meeting current challenges in toxicity testing *Crit. Rev. Toxicol.* **42** 501–48
- [21] van Midwoud P M, Merema M T, Verpoorte E and Groothuis G M 2010 A microfluidic approach for *in vitro* assessment of interorgan interactions in drug metabolism using intestinal and liver slices *Lab Chip* **10** 2778–86
- [22] Slaughter B V, Khurshid S S, Fisher O Z, Khademhosseini A and Peppas N A 2009 Hydrogels in regenerative medicine *Adv. Mater.* **21** 3307–29
- [23] He J, Mao M, Liu Y, Shao J, Jin Z and Li D 2013 Fabrication of nature-inspired microfluidic network for perfusable tissue constructs *Adv. Healthc. Mater.* **2** 1108–13
- [24] Tsang V L et al 2007 Fabrication of 3D hepatic tissues by additive photopatterning of cellular hydrogels *FASEB J.* **21** 790–801
- [25] Li C Y, Stevens K R, Schwartz R E, Alejandro B S, Huang J H and Bhatia S N 2014 Micropatterned cell–cell interactions enable functional encapsulation of primary hepatocytes in hydrogel microtissues *Tissue Eng. A* **20** 2200–12
- [26] Mahto S K, Yoon T H and Rhee S W 2010 A new perspective on *in vitro* assessment method for evaluating quantum dot toxicity by using microfluidics technology *Biomicrofluidics* **4** 034111
- [27] Esch M B et al 2015 Multi-cellular 3D human primary liver cell culture elevates metabolic activity under fluidic flow *Lab Chip* **15** 2269–77
- [28] Liu W et al 2014 Magnetically controllable 3D microtissues based on magnetic microcryogels *Lab Chip* **14** 2614–25
- [29] Moraes C, Labuz J M, Leung B M, Inoue M, Chun T H and Takayama S 2013 On being the right size: scaling effects in designing a human-on-a-chip *Integr. Biol. (Camb.)* **5** 1149–61
- [30] Bertassoni L E et al 2014 Direct-write bioprinting of cell-laden methacrylated gelatin hydrogels *Biofabrication* **6** 024105
- [31] Murphy S V and Atala A 2014 3D bioprinting of tissues and organs *Nat. Biotechnol.* **32** 773–85
- [32] Lee S-A, No D Y, Kang E, Ju J, Kim D-S and Lee S-H 2013 Spheroid-based three-dimensional liver-on-a-chip to investigate hepatocyte-hepatic stellate cell interactions and flow effects *Lab Chip* **13** 3529–37
- [33] Tostoes R M et al 2012 Human liver cell spheroids in extended perfusion bioreactor culture for repeated-dose drug testing *Hepatology* **55** 1227–36
- [34] Thoma C R, Zimmermann M, Agarkova I, Kelm J M and Krek W 2014 3D cell culture systems modeling tumor growth determinants in cancer target discovery *Adv. Drug Deliv. Rev.* **69–70** 29–41
- [35] Karp J M et al 2007 Controlling size, shape and homogeneity of embryoid bodies using poly(ethylene glycol) microwells *Lab Chip* **7** 786–94
- [36] Tung Y C, Hsiao A Y, Allen S G, Torisawa Y S, Ho M and Takayama S 2011 High-throughput 3D spheroid culture and drug testing using a 384 hanging drop array *Analyst* **136** 473–8
- [37] Zhang Y S, Choi S-W and Xia Y 2013 Inverse opal scaffolds for applications in regenerative medicine *Soft Matter* **9** 9747–54
- [38] Haussinger D 1988 Hepatic sublobular synthesis of urea: control by oxygen or by pH gradient? *Hepatology* **8** 184–6
- [39] Nichol J W, Koshy S T, Bae H, Hwang C M, Yamanlar S and Khademhosseini A 2010 Cell-laden microengineered gelatin methacrylate hydrogels *Biomaterials* **31** 5536–44
- [40] Mattei G, Giusti S and Ahluwalia A 2014 Design criteria for generating physiologically relevant *in vitro* models in bioreactors *Processes* **2** 548–69
- [41] Weise F, Fernekorn U, Hampl J, Klett M and Schober A 2013 Analysis and comparison of oxygen consumption of HepG2 cells in a monolayer and three-dimensional high density cell culture by use of a matrigrid® *Biotechnol. Bioeng.* **110** 2504–12
- [42] Buchwald P 2009 FEM-based oxygen consumption and cell viability models for avascular pancreatic islets *Theor. Biol. Med. Modelling* **6** 5
- [43] Ouattara D A et al 2012 Metabolomics-on-a-chip and metabolic flux analysis for label-free modeling of the internal metabolism of HepG2/C3A cells *Mol. Biosyst.* **8** 1908–20
- [44] Tamayol A, Khosla A, Gray B L and Bahrami M 2012 Creeping flow through ordered arrays of micro-cylinders embedded in a rectangular minichannel *Int. J. Heat Mass Transfer* **55** 3900–8
- [45] Luiz E B et al 2014 Direct-write bioprinting of cell-laden methacrylated gelatin hydrogels *Biofabrication* **6** 024105
- [46] Fukuda J et al 2003 Efficacy of a polyurethane foam/spheroid artificial liver by using human hepatoblastoma cell line (Hep G2) *Cell Transplant* **12** 51–8
- [47] Sakai Y and Nakazawa K 2007 Technique for the control of spheroid diameter using microfabricated chips *Acta. Biomater.* **3** 1033–40
- [48] Fraczek J, Bolleyn J, Vanhaecke T, Rogiers V and Vinken M 2013 Primary hepatocyte cultures for pharmacotoxicological studies: at the busy crossroad of various anti-differentiation strategies *Arch. Toxicol.* **87** 577–610
- [49] Ho W J et al 2010 Incorporation of multicellular spheroids into 3D polymeric scaffolds provides an improved tumor model for screening anticancer drugs *Cancer Sci.* **101** 2637–43
- [50] Nichol J W, Koshy S T, Bae H, Hwang C M, Yamanlar S and Khademhosseini A 2010 Cell-laden microengineered gelatin methacrylate hydrogels *Biomaterials* **31** 5536–44
- [51] Billiet T, Gevaert E, De Schryver T, Cornelissen M and Dubruel P 2014 The 3D printing of gelatin methacrylamide cell-laden tissue-engineered constructs with high cell viability *Biomaterials* **35** 49–62
- [52] Chen Y C et al 2012 Functional human vascular network generated in photocrosslinkable gelatin methacrylate hydrogels *Adv. Funct. Mater.* **22** 2027–39

- [53] Kim H N, Kang D H, Kim M S, Jiao A, Kim D H and Suh K Y 2012 Patterning methods for polymers in cell and tissue engineering *Ann. Biomed. Eng.* **40** 1339–55
- [54] Lin J H 2006 CYP induction-mediated drug interactions: in vitro assessment and clinical implications *Pharm. Res.* **23** 1089–116
- [55] Hewitt N J et al 2007 Primary hepatocytes: current understanding of the regulation of metabolic enzymes and transporter proteins, and pharmaceutical practice for the use of hepatocytes in metabolism, enzyme induction, transporter, clearance, and hepatotoxicity studies *Drug Metab. Rev.* **39** 159–234
- [56] Obach R S 2009 Predicting drug-drug interactions from *in vitro* drug metabolism data: challenges and recent advances *Curr. Opin. Drug Discovery Dev.* **12**(1) 81–9
- [57] Gomez-Lechon M J, Donato M T, Castell J V and Jover R 2003 Human hepatocytes as a tool for studying toxicity and drug metabolism *Curr. Drug Metab.* **4** 292–312
- [58] Jennen D G, Magkoufopoulou C, Ketelslegers H B, van Herwijnen M H, Kleinjans J C and van Delft J H 2010 Comparison of HepG2 and HepaRG by whole-genome gene expression analysis for the purpose of chemical hazard identification *Toxicol. Sci.* **115** 66–79
- [59] Wilkening S, Stahl F and Bader A 2003 Comparison of primary human hepatocytes and hepatoma cell line Hepg2 with regard to their biotransformation properties *Drug Metab. Dispos.* **31** 1035–42
- [60] Shan J et al 2013 Identification of small molecules for human hepatocyte expansion and iPS differentiation *Nat. Chem. Biol.* **9** 514–20
- [61] Dash A et al 2013 Hemodynamic flow improves rat hepatocyte morphology, function, and metabolic activity *in vitro* *Am. J. Physiol. Cell Physiol.* **304** C1053–63
- [62] Wagner I et al 2013 A dynamic multi-organ-chip for long-term cultivation and substance testing proven by 3D human liver and skin tissue co-culture *Lab Chip* **13** 3538–47
- [63] Torisawa Y S, Takagi A, Nashimoto Y, Yasukawa T, Shiku H and Matsue T 2007 A multicellular spheroid array to realize spheroid formation, culture, and viability assay on a chip *Biomaterials* **28** 559–66
- [64] Kim M S, Yeon J H and Park J K 2007 A microfluidic platform for three-dimensional cell culture and cell-based assays *Biomed. Microdevices.* **9** 25–34
- [65] Bouma M E, Rogier E, Verthier N, Labarre C and Feldmann G 1989 Further cellular investigation of the human hepatoblastoma-derived cell line HepG2: morphology and immunocytochemical studies of hepatic-secreted proteins. *In Vitro Cell. Developmental Biol. : J. Tissue Cult. Assoc.* **25** 267–75
- [66] Uludag H and Sefton M V 1993 Microencapsulated human hepatoma (HepG2) cells: *in vitro* growth and protein release *J. Biomed. Mater. Res.* **27** 1213–24
- [67] Carraro A et al 2008 *In vitro* analysis of a hepatic device with intrinsic microvascular-based channels *Biomed. Microdevices* **10** 795–805
- [68] Iwasa F, Galbraith R A and Sassa S 1990 Phenotypic variation in human HepG2 hepatoma cells: alterations in cell growth, plasma protein synthesis and heme pathway enzymes *Int. J. Biochem.* **22** 303–10
- [69] van Eyken P, Sciote R, Callea F, van der Steen K, Moerman P and Desmet V J 1988 The development of the intrahepatic bile ducts in man: a keratin-immunohistochemical study *Hepatology* **8** 1586–95
- [70] Treyer A and Musch A 2013 Hepatocyte polarity *Compr. Physiol.* **3**(1) 243–87
- [71] Blazer D G and Wu L T 2009 Nonprescription use of pain relievers by middle-aged and elderly community-living adults: national survey on drug use and health *J. Am. Geriatrics Soc.* **57** 1252–7
- [72] Davidson D G and Eastham W N 1966 Acute liver necrosis following overdose of paracetamol *Br. Med. J.* **2** 497–9
- [73] Fey S J and Wrzesinski K 2012 Determination of drug toxicity using 3D spheroids constructed from an immortal human hepatocyte cell line *Toxicol. Sci.* **127** 403–11
- [74] Allen J W and Bhatia S N 2003 Formation of steady-state oxygen gradients *in vitro*: application to liver zonation *Biotechnol. Bioeng.* **82** 253–62
- [75] Kostadinova R et al 2013 A long-term three dimensional liver co-culture system for improved prediction of clinically relevant drug-induced hepatotoxicity *Toxicology Appl. Pharmacology* **268** 1–16
- [76] Bhatia S N, Underhill G H, Zaret K S and Fox I J 2014 Cell and tissue engineering for liver disease *Sci. Translational Med.* **6** 245sr2
- [77] Maschmeyer I et al 2015 A four-organ-chip for interconnected long-term co-culture of human intestine, liver, skin and kidney equivalents *Lab Chip* **15** 2688–99
- [78] Maschmeyer I et al 2015 Chip-based human liver-intestine and liver-skin co-cultures—a first step toward systemic repeated dose substance testing *in vitro* *Eur. J. Pharmaceutics Biopharmaceutics : Official J. Arbeitsgemeinschaft Pharmazeutische Verfahrenstechnik eV* **95**(Pt A) 77–87